Journal of Crystal Growth 475 (2017) 70–76

Contents lists available at ScienceDirect

Journal of Crystal Growth

journal homepage: www.elsevier.com/locate/crys

In-situ detection of growth striations by crystallization electromotive force measurement during Czochralski crystal growth

Yunzhong Zhu [a], Decai Ma [a], Siwei Long [b], Feng Tang [b], Shaopeng Lin [a,*], Biao Wang [a,b,*]

[a] Sino French Institute of Nuclear Engineering and Technology, Sun Yat-sen University, Zhuhai 519082, China
[b] State Key Laboratory of Optoelectronic Materials and Technologies/Institute of Optoelectronic and Functional Composite Materials, School of Physics and Engineering, Sun Yat-sen University, Guangzhou 510275, China

ARTICLE INFO

Article history:
Received 15 April 2017
Received in revised form 20 May 2017
Accepted 24 May 2017
Available online 25 May 2017
Communicated by P. Rudolph

Keywords:
A1. Defects
A1. Interfaces
A2. Czochralski method
B1. Lithium compounds
B1. Niobates
B1. Oxides

ABSTRACT

Growth striations, as macrodefects of crystalline materials, are mainly caused by convection and temperature fluctuations in growth interface. For decades, striations have been widely regarded as an inherent problem. Even in the well-developed Czochralski method, the striation formation process is difficult to inspect in situ. In view of this long-standing issue, after systematically studying the temperature, weight, and output power during crystal growth and numerically modeling the growth process, we found that the regularity of the growth interface electromotive force (GEMF) is related to the distribution of striations. Furthermore, the GEMF quantifies interface fluctuations (711.2 s, 16.6 μm) and thermal hysteresis (107 s), presenting finer details than those provided by a thermocouple and a load cell. In this paper, GEMF is found to be an outstanding choice for monitoring the crystal growth status in real time. As an additional feedback, a new automatic control method could be developed for reducing growth striations and promoting crystal quality.

© 2017 Elsevier B.V. All rights reserved.

1. Introduction

Despite recent progress in crystal growth techniques and the great dependence upon macroscopic crystalline materials in the sci-tech field, the growth of extremely homogeneous crystals is still challenging. However, inhomogeneous solutes usually appear as growth striations. As an inherent problem [1], striations are essentially formed by spasmodic growth-rate variation [2–4] that directly correlates with convection and temperature fluctuations. In addition, as macrodefects of crystals, growth striations represent insufficient quality. Specifically, striations can be divided into thermal (including rotational striation) [5], macrostep-induced [6], and instability-induced striations [1]. They are common problems encountered in crystal growth that can be reduced but not eradicated. To approach striation-free crystal growth conditions, researchers have experimented with external fields such as ultrasound, magnetic fields, and even microgravity to suppress temperature and convection fluctuations [4,7–11]. However, constrained by the prolonged growth time of a single crystal and the changeable growth environment, research involving growth striations requires considerable patience. Usually, the results of each modulation parameter can only be acquired at the end of the growth cycle. Acquiring a single complete set of data may require months of consecutive experiment, which makes such research scarce and valuable. Obviously, the aforementioned works represent remarkable progress; however, none of them has eradicated growth striations. Therefore, reducing striations has become a continuous and costly pursuit in crystal industry. Although methods to reduce growth striations have been developed, the in-situ feedback of striation formation process would dramatically shorten the research cycle and have a tremendous impact.

This paper presents a method to analyze thermal striations in real time during the Czochralski (CZ) crystal growth of congruent lithium niobate (CLN). The formation process of striations is revealed via electrical studies of the growth interface. The mainstream automatic crystal growth method is well known to depend on temperature, weight or image recognition. The automatic body control of the as-grown crystal is achieved via a high-temperature thermocouple and a high-precision load cell. In CZ method, a thermocouple positioned beside the crucible cannot accurately reflect the temperature of the growth interface; thus, the correlated output power (OP) does not represent the optimal response. Such a mechanism imperfection may induce an undetectable temperature deviation in growth interface. However, in practice, installing an additional contact transducer in growth interface is unrealistic.

* Corresponding authors at: Sino French Institute of Nuclear Engineering and Technology, Sun Yat-sen University, Zhuhai 519082, China (S. P. Lin and B. Wang).
E-mail addresses: lshpeng@mail.sysu.edu.cn (S. Lin), wangbiao@mail.sysu.edu.cn (B. Wang).

http://dx.doi.org/10.1016/j.jcrysgro.2017.05.026
0022-0248/© 2017 Elsevier B.V. All rights reserved.

On the other hand, the non-contact measurement cannot meet the level of rigor for crystal growth. Even the newly applied image recognition method (charge-coupled device, CCD) [12,13] can only present the crystal outline rather than the interface between the solid and the melt. In addition to a thermocouple and a CCD, a load cell is another standard configuration of current CZ equipment. Subjected to the load range and resolution, the chosen load cell already possesses the highest resolution (10 mg). Unfortunately, it can barely detect tiny weight changes such as striation formation. Given the aforementioned considerations, the accurate observation of growth interface would appear to be unobtainable. Nonetheless, because of the critical role of growth interface in the occurrence of growth striations, the in-situ detection of growth interface is currently a key issue in crystal industry.

To solve this problem, we have delved into an interesting phenomenon in which an electromotive force (EMF) is generated in the growth interface of CLN [14,15]. On the basis of well-developed high-temperature Raman spectroscopy techniques, the growth interface has been revealed to a thickness of microns, detailing gradual changes in the microstructure [16,17]. To control the domain and segregation coefficient, researchers previously investigated the growth interface under an external electric field [18,19]. In that case, the intrinsic EMF is regarded as a negligible attachment. However, it plays the major role in the present work. We have found a periodic potential fluctuation signal in the growth interface electromotive force (GEMF, ϕ_{GE}). More interestingly, the formation of growth striations and feeble fluctuations of OP, which are undetectable by a thermocouple and a load cell, are closely related to this periodic signal. As indicated in the literature [15,20,21], GEMF is generated from the partitioning of oppositely charged valence ions on both sides of the growth interface (crystallization EMF, CEMF, ϕ_{CE}) and from the thermoelectromotive force produced by the solid and liquid phases (thermal EMF, ϕ_{tho}) [15]. Specially, ϕ_{tho} is consist of the supercooling electromotive force (SEMF, ϕ_{scl}) in growth interface and the Seebeck potential (ϕ_{sbk}) between crystal and melt [21]:

$$\phi_{GE} = \phi_{tho} + \phi_{CE} \quad (1)$$

$$\phi_{tho} = \phi_{sbk} + \phi_{scl} \quad (2)$$

This electric potential is frequently used to calculate and manipulate the segregation coefficient [22,23]; however, it barely reveals striations and the condition of the crystal growth interface. According to the strong correlation between the GEMF and the core position of a growing crystal, and with the assistance of numerical modeling, we deduced some important factors, including interface fluctuations, transient growth speed and thermal hysteresis. Moreover, based on this discovery, the in-situ feedback of growth striations (which cannot be probed by image recognition, weight or temperature methods) could be realized. In summary, the purpose of the present work is to experimentally demonstrate a feasible method for describing the growth striations using GEMF.

2. Materials and methods

2.1. Growth of lithium niobate single crystals

High-purity CLN raw materials were prepared from Li_2CO_3 (99.99% purity) and Nb_2O_5 (99.99% purity) powders. They were mixed and ball milled uniformly in a Li/Nb molar ratio of 0.946 and subsequently heated at 1250 °C for 24 h in a muffle furnace. The crystal was then grown by the self-developed automatic CZ system. The system can automatically grow a crystal and simultaneously record the temperature, OP, weight data, and other basic parameters.

2.2. Electromotive force characterization

In conjunction with the automatic crystal growth furnace, one additional thermocouple, one multimeter (Keithley 2100) and two platinum electrodes were used to measure the temperature of seed crystal (T_1) and the GEMF between the platinum crucible and the pulling rod (as described in Eq. (1)). Accordingly, a schematic of crystal growth and the GEMF measurement platform is presented in Fig. 1a. A 15 mm long seed crystal was selected on the *c*-axis. The diameter of the as-grown crystal was automatically maintained at 20 mm. During the whole crystal growth process, the pulling rate was 5 mm/h, the rotation rate was 15 rpm, and the GEMF measurements were collected simultaneously. Combining Fig. 1a and b, the ϕ_{GE}-T_1 curve starts in point *a*, a normal crystal

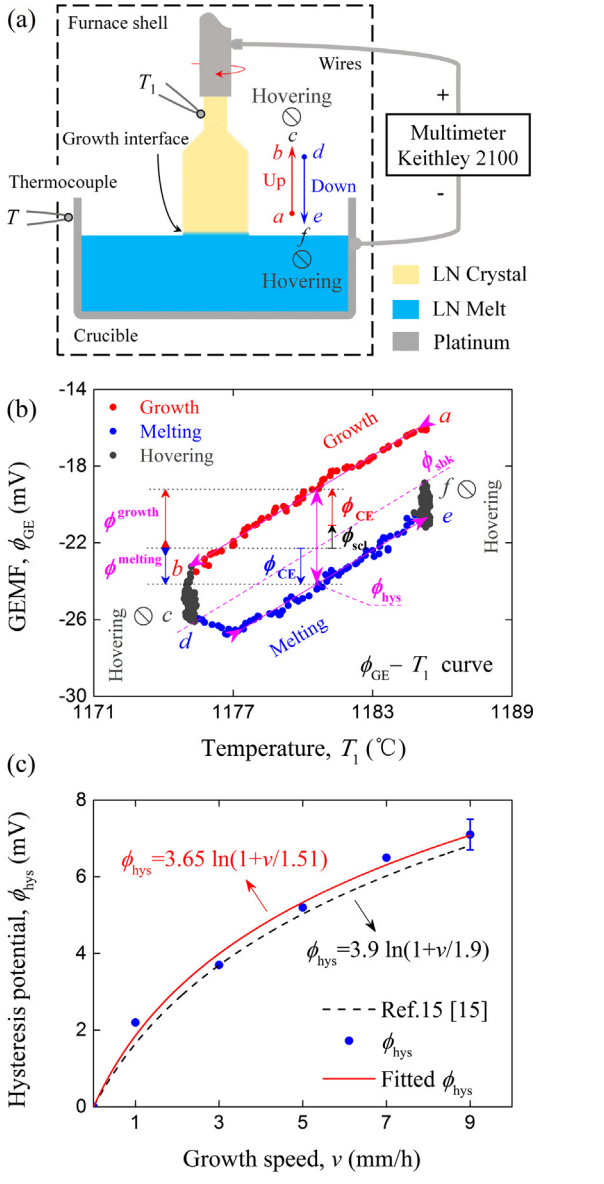

Fig. 1. (a) Schematic of the experimental platform. The potential (φ_{GE}) between the platinum pulling rod and crucible was measured using a multimeter. (b) The φ_{GE}-T_1 curve during the process of growth, hovering and melting. The crystallization EMF (φ_{CE}) and supercooling EMF (φ_{scl}) can be obtained from the hysteresis potential (φ_{hys}). (c) The measured φ_{hys} versus different growth speed (v = 1, 3, 5, 7, 9 mm/h). The red solid line presents the fitted formula of the experiment results, where φ_0 = 3.65 mV and v_0 = 1.51 mm/h. The black dash line presents the formula in Ref. [15]. (For interpretation of the references to colour in this figure legend, the reader is referred to the web version of this article.)

growth moment. From point *a* to *b*, the crystal keeps pulling up in 5 mm/h for 4 h as usual. Then we stop pulling in point *b*. Right after stopping, GEMF flattens out gradually in an hour after a steep fall (point *c*). One hour later, the pushing down operation starts in the same speed (point *d*). Meanwhile, GEMF changes rapidly, and then keeps a steady slope for 4 h until the crystal stops again (point *e*). In the period from pulling up to pushing down, the direction of ϕ_{CE} reverses, because the crystal changes from crystallization to melting. As described above, after a reciprocating motion, the crystal reaches back to the initial position. Point *f* is the stopping point accompanied by a rapid GEMF increase. Then just like point *c*, GEMF flattens out in an hour again. Up to this point, the ϕ_{GE} hysteresis loop of specific growth speed has been drawn in Fig. 1b. The width of the ϕ_{GE}-T_1 curve is defined as the hysteresis potential (ϕ_{hys}), which is the key clue to study ϕ_{GE}. Moreover, similar "round-trip" processes have been investigated in different growth speed (v = 1, 3, 5, 7, 9 mm/h) as well; and each $\phi_{hys}(v)$ has been plotted in Fig. 1c. The types of EMF and the fitting results in Fig. 1b and 1c will be discussed in details as follows, respectively.

2.3. Computer modeling

Computer models were used to study heat transfer under OP oscillations. The simulation results were considered within the conjugated 2D/3D numerical approach by the reliable commercial program Crystal Growth Simulator (CGSim). This program has been used to simulate crystal growth conditions successfully, especially for the CZ method [24–26].

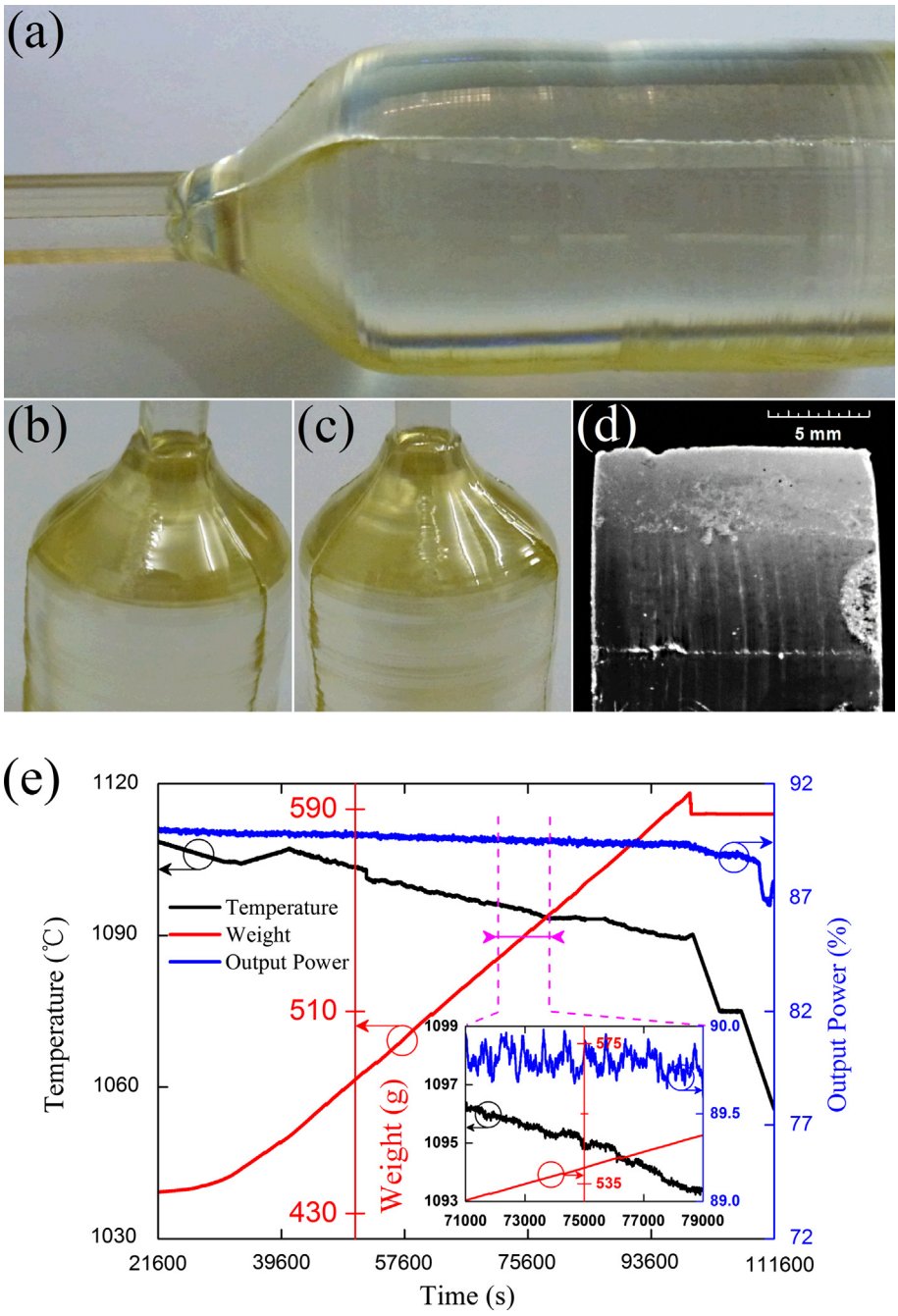

Fig. 2. (a–d) Photograph of the as-grown CLN single crystal. (d) The partial enlarged view of the crystal surface. (e) Data record of temperature, weight and output power during the entire crystal growth process. The inset of Fig. 2e is the data record corresponding to Fig. 2d.

3. Results and discussion

Striations are undetectable macrodefects that occur during crystal growth. To confirm this viewpoint, the bulk CLN sample is shown in Fig. 2a–d. The uniform cylinder shape, standard crystallization angle, and three symmetrical ridges imply that the as-grown CLN grew via a perfect crystal growth process. Moreover, from the data record (temperature, weight and OP) of the entire growth process in Fig. 2e, the normal feedback data of the thermocouple, load cell, and power source demonstrate a stable "shoulder" and "body" growth process, as well. Specifically, Fig. 2e shows a smooth weight curve, steady temperature control and small power fluctuations. Actually, the inset of Fig. 2e which is the data record corresponding to Fig. 2d, presents a standard control process. In general, all of the growth parameters appear to be maintained under perfect control.

However, the well-performed growth process dramatically highlights the appearance of striations. As shown in Fig. 2d, which is an annealed and polarized longitudinal cutting chip of the crystal surface, the regular and continuous striations are observed on the surface of the CLN and are mainly parallel to the crystallization front, with an average spacing of 974.5 μm. Therefore, on the basis of the results of Fig. 2a–e, one can come to the conclusion that, because of the absence of striation detection in conventional method, the striation reduction studies lack sufficient sensitivity. Thus, we select GEMF to solve the difficult problem of detecting the striation formation process in growth interface.

We here describe our adoption of GEMF to characterize the growth interface. Fig. 3 shows a plot of the GEMF record for the same period as that represented in Fig. 2d and reveals an obvious regular fluctuation signal. Similar signals are observed neither in the temperature record nor in the weight record (see Fig. 2e) because the temperature is usually measured at the crucible edge, which is relatively far from the growth interface. Moreover, in the thermal insulation system, convections complicate the heat exchange. In such a temperature field, all these factors impede an accurate feedback of the temperature of the crystal growth interface from the thermocouple. The load cell performs similarly and it is insensitive to the tiny mass changes that accompany the formation of growth striations. In Fig. 3, the fluctuation range (0.2%) of OP record completely satisfies the requirements of crystal growth. Moreover, after sine fitting, we still obtain a regular OP curve (red solid line in Fig. 3, T_{OP} = 705.4 s). The GEMF oscillates periodically in accordance with the fitted OP, which demonstrates that the feeble power fluctuation is the source of the GEMF fluctuation. More interestingly, according to the macroscopic growth speed (5 mm/h) and the fitted fluctuation period (T_{OP}), the pulling "wavelength" could be calculated as λ = 979.7 μm. Coincidentally, this wavelength is highly consistent with the average spacing (974.5 μm) of growth striations in Fig. 2d, which implies a direct relationship among the OP, the GEMF and the striations. This novel and regular phenomenon has attracted great attention. In fact, growth striations and GEMF fluctuations are two types of external manifestations of growth speed variation. It is known that the striation is effected by the variations of both temperature and melt convection, which are induced by OP fluctuation. For different materials and temperature field, these two factors have different influence extent and vary the growth speed at the same time. Besides striation, another external performance of growth speed variation is GEMF. As shown in Eqs. (1) and (2), CEMF and SEMF are important components of GEMF. These two kinds of EMF are essentially controlled by the segregation, redistribution and solute transport phenomenon of ionic species [20], and supercooling degree [21], respectively. These physics phenomenon could be generally considered as mass transport at growth interface. Obviously, the accumulation of mass transport presents the macro mass change of crystal. Therefore, GEMF could also reflect growth speed intuitively.

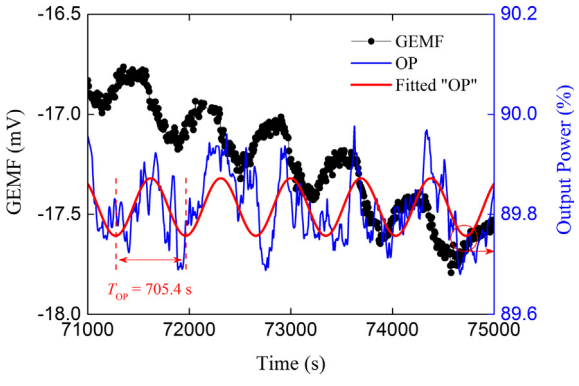

Fig. 3. The GEMF and output power (OP) record corresponding to the period in the inset of Fig. 2e. The red solid curve presents the sine-fitted output power data, which exhibits a period of 705.4 s. (For interpretation of the references to colour in this figure legend, the reader is referred to the web version of this article.)

The GEMF consists of two different types of electromotive force, thus, to study the regular phenomenon of GEMF further, the roles of ϕ_{CE}, ϕ_{scl} and ϕ_{sbk} must be examined. First, the effect of the slight power fluctuation during crystal growth has to be revealed. In Fig. 4a-c, the numerical modeling temperature field of the power fluctuation is presented. Although the temperature simulation of particular location in growth system cannot be accurate, the reflection of variation trend and relative change is reliable. Thus, Fig. 4b and 4c show the temperature change of particular locations (i.e., the interface of the melt, and the interface between the melt and crucible, respectively) under different output power (OP- and OP + correspond to -0.1% and + 0.1%). In Fig. 4b and 4c, the numerical simulation results represent the stable growth condition of specific OP. As the seed temperature kept constant, the temperature of the free melt surface changes with a magnitude of 0.130 K, and the temperature of the interface between melt and crucible changes 0.194 K. Obviously, unlike the stable condition, in the case of thermal conduction and convection, the transient rangeability of temperature variation in the period of 705.4 s is less than the simulation results. Furthermore, for the quasistatic process during crystal growth, the Seebeck potential can be expressed as,

$$\phi_{sbk} = \alpha_L(T_2 - T_0) + \alpha_S(T_0 - T_1) \quad (3)$$

where α_L = 0.23 mV/K and α_S = −0.71 mV/K are the Seebeck coefficients of the CLN liquid and solid phases, respectively; T_0, T_1 and T_2 represent the temperature of the growth interface, the seed crystal and the melt, respectively [20]. Based on Eq. (3) and the numerical simulation results, the maximum ϕ_{sbk} fluctuation under the power oscillation of 0.2% reached 0.04 mV. Meanwhile, the Seebeck coefficient of platinum is α_{Pt} = 0.025 mV/K [15]; referring to Fig. 2e, the irregular and tiny temperature fluctuation of the platinum crucible cannot generate a regular and significant Seebeck signal. Therefore, in conclusion, the numerical and experimental results demonstrate that ϕ_{sbk} contributes little to the GEMF fluctuation of 0.38 mV (as shown in Fig. 3). Thus, we infer that the periodic fluctuation of GEMF is mainly caused by the crystallization electromotive force and the supercooling electromotive force in growth interface. The ϕ_{CE} and ϕ_{scl} are both directly related to the crystal growth speed (v) and remains relatively constant at any crystal length [14,15,21].

For exploring the phenomenon accurately, ϕ_{CE} and ϕ_{scl} must be extracted from GEMF, where the ϕ_{hys} and the asymmetry of ϕ_{GE}-T_1 curve may play important roles. The relationship between ϕ_{hys} and

crystal growth speed (v) had been investigated by semiconductive model [15],

$$\phi_{hys} = \phi_0 \ln(1 + v/v_0) \quad (4)$$

where ϕ_0 and v_0 are system dependent coefficients. To achieve an accurate $\phi_{hys}(v)$ formula, the ϕ_{hys} in different growth speed (v = 1, 3, 5, 7, 9 mm/h) are plotted in Fig. 1c. The ϕ_{hys} versus v points are well fitted by Eq. (4); then the coefficients ϕ_0 = 3.65 mV and v_0 = 1.51 mm/h are obtained. In Fig. 1c, compared with Aleksandrovskii and Shumov's work (ϕ_0 = 3.9 mV and v_0 = 1.9 mm/h) [15], the similar fitted results may imply the similar CZ growth system.

On the other hand, when crystal stops pulling up or pushing down, there is no SEMF and CEMF in GEMF [21]. Then the ϕ_{sbk} becomes the only surviving electric signal between the crystal and melt. For this reason, in Fig. 1b, the connection line of both ends of the ϕ_{GE}-T_1 curve (point "*e* to *f*") separates the GEMF of growth and melting process. Then the EMF generated from crystal growth and melting could be measured as ϕ^{growth} = 3.1 mV and $\phi^{melting}$ = −1.9 mV (v = 5 mm/h). These results are similar to the test results of Koh and Uda via micro-pulling method (ϕ^{growth} = 3.7 mV, $\phi^{melting}$ = −2.3 mV, v = 5 mm/h) [20]. Although the CEMF in growth and melting process are slightly different because of the Seebeck potential [20] and the different behavior of ionic species between solidification and melting, the simplification of identical growth and melting CEMF absolute value are frequently used [20,27–29]. Since the segregation is regarded to take place in opposite manner during growth and melting [29]; and because of this, we assume $|\phi_{CE(growth)}| = |\phi_{CE(melting)}| = \phi_{CE}$ for simplicity as well. Then, in ϕ_{GE}-T_1 curve, we can attribute the asymmetric of the electric potential generated by pulling up and down operation (ϕ^{growth} and $\phi^{melting}$) to the existent of ϕ_{scl},

$$|\phi^{growth}| - |\phi^{melting}| = \phi_{scl} \quad (5)$$

$$\phi_{scl} = A \times v \quad (6)$$

where A is a coefficient directly related to supercooling degree [21]. Thus, we have confirmed the linear relationship between ϕ_{scl} and growth speed. However, there is a huge difference in the temperature gradient of CZ and micro-pulling method (more than 1000 °C/cm), which results in a different supercooling degree. Based on Eq. (6) and the measured ϕ_{scl} (1.2 mV) in Fig. 1b, the coefficient A should be 0.24 mV h/mm, and this result is close to the supercooling degree measurement and in-situ growth rate observation of $LiNbO_3$ by Jin and Tsukamoto (A = 0.21 mV h/mm) [30].

In ϕ_{GE}-T_1 curve, the hysteresis potential represents a sum of ϕ^{growth} and $\phi^{melting}$. Thus, ϕ_{hys} can be expressed as,

$$\phi_{hys} = \phi_{scl} + 2\phi_{CE} \quad (7)$$

Based on the results discussed above and the round-trip experiment in Fig. 1; employing Eq. (4)–(7), the EMF generated by crystal growth operation could be established as,

$$\phi^{growth} = [\phi_0 \ln(1 + v/v_0) + A \times v]/2 \quad (8)$$

Thus, the crystal growth speed (v) becomes the only variable.

As shown in Eqs. (1) and (2), GEMF is the sum of ϕ_{CE}, ϕ_{sbk} and ϕ_{scl}. During the CZ crystal growth process, ϕ_{sbk} is mainly related to the pulling height and contributes to the slope of the GEMF curve [27]. Moreover, on the basis of the calculated ϕ^{growth} = 3.25 mV (v = 5 mm/h) in Eq. (8), we can translate ϕ^{growth} from the ϕ_{GE} as the plotted black curve (crystal growth EMF) in Fig. 5. The macroscopic growth speed is known to equal the pulling rate. However, the growing crystal behaves as a cylinder pulled from continuous waves of molten liquid. That is, the growth interface oscillates the accurate growth speed in each short period [2]. For further analysis of growth striations, the mechanisms of both ϕ^{growth} and the growth speed fluctuation are central to the following discussion.

In addition to the crystal growth EMF curve, Fig. 5 also shows the corresponding transient growth speed calculated from ϕ^{growth} via Eq. (8). The blue dotted speed curve clarifies the transient growth speed. Moreover, in this particular process, the temperature remains stable (see Figs. 2e and 4). That is, the inducement of growth speed fluctuation is the periodic interface undulation caused by power fluctuation. Specifically, in Fig. 5, the calculated growth speed curve represents the relative motion between the growing crystal and the growth interface. To our knowledge, the

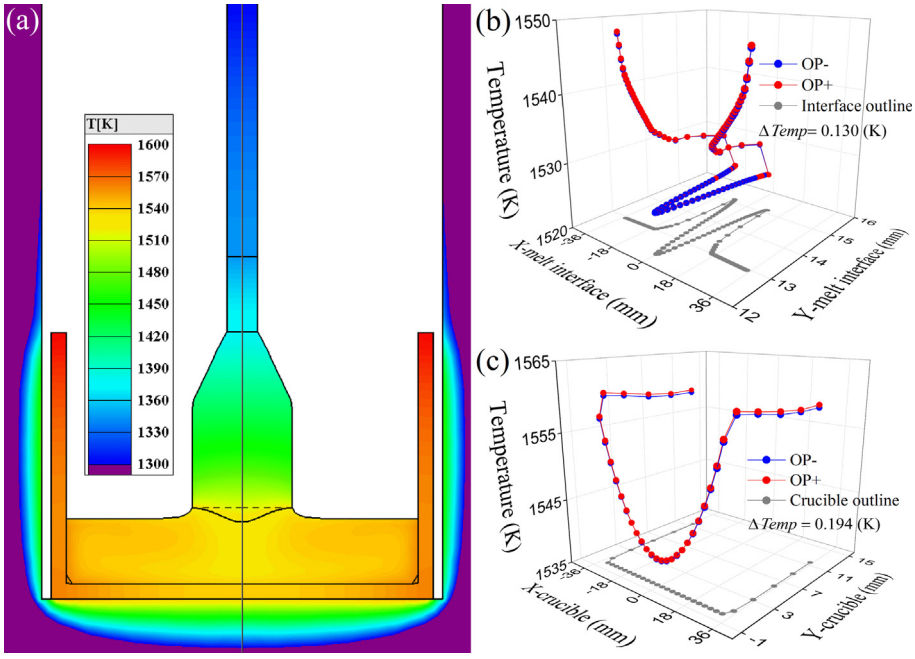

Fig. 4. (a) The computational temperature field of the entire growth system. (b and c) The corresponding temperature fields of different output power (OP) in the interface of the melt and in the interface between the melt and the crucible. The OP− and OP+ curves correspond to percentage power deviations of −0.1% and +0.1%, respectively.

relatively high Prandtl number (13.6) of lithium niobate [31,32] implies that the liquid convection is the main spread medium of the fluctuation phenomenon. Hence, the growth speed fluctuation can be regarded as waves in the melting lithium niobate. These "waves" oscillate the growth interface periodically and leave striations on the crystal every 979.7 μm (close to the observed striation spacing of 974.5 μm). The growth striation investigated in this paper also could be regarded as thermal striation. However, differ from common thermal striation, the power fluctuation does not produce a detectable and regular temperature fluctuation. But by using a less-visible way, the fluctuation of OP transmits to growth interface via the hydrodynamic flow, and varies the growth speed at the same time. The periodic GEMF fluctuation could be concluded as the team performance of both CEMF and SEMF, resulting from the variation of growth speed due to the OP variation. In short, the regular growth interface fluctuation vibrated by power fluctuation is the origin of growth striations.

At this point, the quantitative study of the growth interface fluctuation can be taken further. In Fig. 5, the growth speed curve is sine-fitted as the blue solid line. It possesses a period of T_V = 711.2 s and an integral area of 16.6 μm (red translucent area). As expected, the period of the fitted growth speed is in accordance with the OP fluctuation (in Fig. 3). However, the more remarkable observation is that the integral area represents the displacement of a single undulation. To be specific, the difference between the fitted transient growth speed (blue solid line) and the average growth speed (red dot line) depicts the movement rule of the growth interface. Obviously, the enclosed area represents the corresponding fluctuation range of 16.6 μm. Thus far, the quantified results make the visual assessment of the crystal growth interface a reality. Notably, the calculated results only represent the condition of the growth interface on average. In practice, either the striation spacing in Fig. 2d or the growth speed in Fig. 5 is not strictly consistent with the periodic arrangement. Although an unstable disturbance still exists in a practical heat-insulation system, it does not affect the average striation distribution or the overall regularity of the GEMF. Obviously, on the basis of the method used in this paper, the study of any targeted thermal striation is feasible.

In the aforementioned process, the fluctuation period of the OP transmits in the order of power source, platinum crucible, molten polycrystalline, liquid convection, growth interface, growth speed variation, and GEMF. Finally, the variation of the periodic GEMF is presented in Fig. 5. Because of the ordinal fluctuation transmission, the period of GEMF is in accord with the power fluctuation.

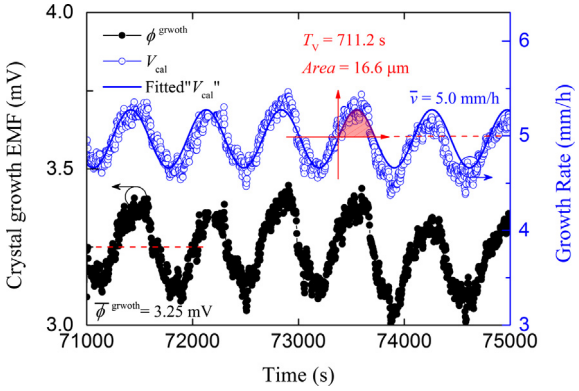

Fig. 5. The calculated crystal growth EMF (φ^{growth}) and the growth speed (V_{cal}) as a function of time. The blue solid curve and red translucent area present the sine-fitted V_{cal} and the integral result, respectively. The red dash lines in the wave curves present the average data of φ^{growth} and the growth speed. (For interpretation of the references to colour in this figure legend, the reader is referred to the web version of this article.)

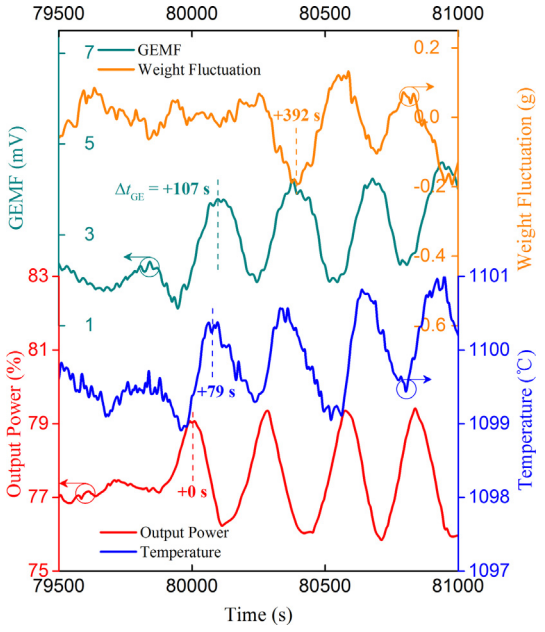

Fig. 6. The affected temperature, weight fluctuation and GEMF record under an artificial output power oscillation. The colored numbers labeled around dotted lines represent the thermal hysteresis time of each sensor.

However, in a thermal insulation system, thermal hysteresis would be generated in each part of the system inevitably. It functions as a phase difference between different curves in the same timeline. To explore the thermal hysteresis phenomenon further, and inspired by previous work [3], we set an artificial OP oscillation in the growing crystal. The affected temperature, weight fluctuation and GEMF performance are shown in Fig. 6, where the thermal hysteresis time of each sensor is represented as colored numbers. During the artificial OP oscillation, the first power peak of a rising trend should correspond to the maximum temperature of crystal growth system and the minimum of the weight fluctuation. More specifically, as noted in Fig. 6, the thermal hysteresis time of GEMF (Δt_{GE} = 107 s) is between that of the thermocouple (79 s) and that of the load cell (392 s), in ascending order. Note that Δt_{GE} is the response time of the growth system to OP. It is the comprehensive performance of the temperature and the crystallization velocity, and the Seebeck potential plays the major role. Obviously, when OP increase sharply (3%, see Fig. 6), the Seebeck potential would also increase significantly. Because when the temperature of growth system increase (including T_1 and T_2), the solid-liquid interface (T_0) keeps constant simultaneously. In this case, by contrast, the value of CEMF and SEMF are relatively small and their influence on ϕ_{CE} is quite limited. As discussed earlier, the inner mechanism of the thermocouple temperature measurement is deficient, because it only reflects a single point of the heat-insulation system. Compared with the thermocouple, the time delay of GEMF is longer; but the GEMF record directly presents the overall state of the growth system. In addition, the load cell could also feedback the growth state visually. However, the limited resolution requires more mass accumulation, which results in a much more lagging response. Therefore, the GEMF provides a good alternative for controlling and optimizing the crystal growth process in real time.

4. Conclusions

According to the analysis of the thermocouple, load cell, OP, GEMF data, and numerical modeling of heat transfer during a crystal growth process, a method to inspect the growth interface in situ

is established. In particular, the GEMF fluctuation accurately quantifies the growth interface fluctuation, thermal hysteresis, and the formation process of growth striations. This work also concludes that the inducement of interface fluctuation is the slight and periodic convection wave caused by power fluctuation; and that the striation is the appearance of a growth interface fluctuation. GEMF provides a good solution for in-situ monitoring crystal growth status. More importantly, as an additional feedback of crystal growth, a new automatic control system could be developed to enhance crystal quality.

Acknowledgment

This work was supported by the National Natural Science Foundation of China (NSFC) (Nos. 11372361, 11302268, 11232015, 11472321, 11572355); the Guangdong Science & Technology Project (2015B090927005); Fundamental Research Funds for the Central Universities and the Doctoral Program of Higher Education of China (20130171130003).

References

[1] H.J. Scheel, Theoretical and technological solutions of the striation problem, J. Cryst. Growth 287 (2006) 214–223.
[2] C. Stelian, T. Duffar, J.L. Santailler, I. Nicoara, Influence of temperature oscillations on the interface velocity during Bridgman crystal growth, J. Cryst. Growth 237 (2002) 1701–1706.
[3] C. Potard, P. Dusserre, T. Duffar, Impurity Striations during Bridgman Growth of InSb, Cryst. Res. Technol. 32 (1997) 925–929.
[4] G.N. Kozhemyakin, L.G. Kolodyazhnaya, Growth striations in Bi-Sb alloy single crystals pulled in the presence of ultrasonic vibrations, J. Cryst. Growth 147 (1995) 200–206.
[5] A.F. Witt, M. Lichtensteiger, H.C. Gatos, Experimental approach to the quantitative determination of dopant segregation during crystal growth on a microscale: Ga doped Ge, J. Electrochem. Soc. 120 (1973) 1119–1123.
[6] H.J. Scheel, Transition to faceting in multilayer liquid phase epitaxy of GaAs, Appl. Phys. Lett. 37 (1980) 70–73.
[7] B. Cockayne, M.P. Gates, Growth striations in vertically pulled oxide and fluoride single crystals, J. Mater. Sci. 2 (1967) 118–123.
[8] G.N. Kozhemyakin, Influence of solid-liquid interface shape on striations during CZ InSb single crystal growth in ultrasonic fields, J. Cryst. Growth 360 (2012) 35–37.
[9] K.S. Choe, Growth striations and impurity concentrations in HMCZ silicon crystals, J. Cryst. Growth 262 (2004) 35–39.
[10] V.I. Strelov, E.N. Korobeynikova, V.I. Folomeev, Control of convective processes in a melt for growth of doped semiconductor crystals with high homogeneity of properties, Cryst. Growth Des. 11 (2010) 69–74.
[11] T. Duffar, M.D. Serrano, L. Lerin, J.L. Santailler, Marangoni convective effect during crystal growth in space, Cryst. Res. Technol. 34 (1999) 457–465.
[12] D. Liu, J. Liang, A Bayesian approach to diameter estimation in the diameter control system of silicon single crystal growth, IEEE Trans. Instrum. Meas. 60 (2011) 1307–1315.
[13] J. Liang, M. Zhang, D. Liu, W. Wang, Shape fitting for the shape control system of silicon single crystal growth, IEEE Trans. Inform. 11 (2015) 363–374.
[14] V.A. D'yakov, D.P. Shumov, L.N. Rashkovich, A.L. Aleksandrovskii, Electrical phenomena accompanying the Czochralski and Stepanov growth of lithium niobate crystals from the melt, Bull. Acad. Sci. USSR, Phys. Ser. 49 (1985) 117.
[15] A.L. Aleksandrovskii, D.P. Shumov, "Crystallization E.M.F". Investigation in the lithium niobate pulling process from the melt, Cryst. Res. Technol. 25 (1990) 1239–1244.
[16] S. Wan, X. Zhang, S. Zhao, Q. Zhang, J. You, L. Lu, P. Fu, Y. Wu, S. Yin, Raman spectroscopy study on CsB_3O_5 crystal-melt boundary layer structure, Cryst. Growth Des. 8 (2008) 412–414.
[17] S. Wan, B. Zhang, Y. Sun, X. Tang, J. You, Structural analyses of a K_2O-rich $KNbO_3$ melt and the mechanism of $KNbO_3$ crystal growth, CrystEngComm 17 (2015) 2636–2641.
[18] A. Feisst, P. Koidl, Current induced periodic ferroelectric domain structures in $LiNbO_3$ applied for efficient nonlinear optical frequency mixing, Appl. Phys. Lett. 47 (1985) 1125–1127.
[19] F. Duan, M. NaiBen, H. JingFen, W. WenShan, Ferroelectric crystals with periodic laminar domains, Ferroelectrics 91 (1989) 9–19.
[20] S. Koh, S. Uda, M. Nishida, H. Xinming, Study of the mechanism of crystallization electromotive force during growth of congruent $LiNbO_3$ using a micro-pulling-down method, J. Cryst. Growth 297 (2006) 247–258.
[21] H. Kimura, S. Uda, Conversion of non-stoichiometry of $LiNbO_3$, to constitutional stoichiometry by impurity doping, J. Cryst. Growth 311 (2009) 4094–4101.
[22] S. Uda, T. Tsubota, Ionic impurity transport and partitioning at the solid-liquid interface during growth of lithium niobate under an external electric field by electric current injection, J. Cryst. Growth 312 (2010) 3650–3657.
[23] Y. Azuma, S. Uda, Electric current induced compositional variation in $LiNbO_3$ fiber crystal grown by a micro-pulling down method, J. Cryst. Growth 306 (2007) 217–224.
[24] X. Li, Y. Liu, B. Wang, Y.Z. Zhu, Global heat loss and thermal stress analysis in Czochralski crystal growth, Cryst. Res. Technol. 49 (2014) 376–382.
[25] O.V. Smirnova, N.V. Durnev, K.E. Shandrakova, E.L. Mizitovb, V.D. Soklakov, Optimization of furnace design and growth parameters for Si Cz growth, using numerical simulation, J. Cryst. Growth 310 (2008) 2185–2191.
[26] K. Mazaev, V. Kalaev, E. Galenin, S. Tkachenko, O. Sidletskiy, Heat transfer and convection in Czochralski growth of large BGO Crystals, J. Cryst. Growth 311 (2009) 3933–3937.
[27] H. Kimura, H. Koizumi, T. Uchida, S. Uda, Influence of impurity doping on the partitioning of intrinsic ionic species during the growth of $LiNbO_3$ crystal from the melt, J. Cryst. Growth 311 (2009) 1553–1558.
[28] S. Koh, S. Uda, X. Huang, Partitioning of ionic species and crystallization electromotive force during the melt growth of $LiNbO_3$ and $Li_2B_4O_7$, J. Cryst. Growth 306 (2007) 406–412.
[29] J. Nozawa, S. Iida, C. Koyama, et al., Partitioning of ionic species during growth of impurity-doped lithium niobate by electric current injection, J. Cryst. Growth 406 (2014) 78–84.
[30] W. Jin, K. Tsukamoto, Anisotropic growth of $LiNbO_3$, crystal as revealed by high temperature in situ observation, J. Cryst. Growth 123 (1992) 327–332.
[31] M.N. Borjini, L. Kolsi, N. Daous, H.B. Aissia, Hydromagnetic double-diffusive laminar natural convection in a radiatively participating fluid, Numer. Heat Tr. A-Appl. 48 (2005) 483–506.
[32] M.N. Borjini, H.B. Aissia, K. Halouani, B. Zeghmati, Effect of optical properties on oscillatory hydromagnetic double-diffusive convection within semitransparent fluid, Int. J. Heat Mass Transf. 49 (2006) 3984–3996.